



**HAL**  
open science

## Effect of Sulfuric Acid Patination Treatment on Atmospheric Corrosion of Weathering Steel

Ana Crespo, Iván Díaz, Delphine Neff, Irene Llorente, Sagrario Martínez-Ramírez, Emilio Cano

► **To cite this version:**

Ana Crespo, Iván Díaz, Delphine Neff, Irene Llorente, Sagrario Martínez-Ramírez, et al.. Effect of Sulfuric Acid Patination Treatment on Atmospheric Corrosion of Weathering Steel. *Metals*, 2020, 10 (5), pp.591. 10.3390/met10050591 . cea-03748551

**HAL Id: cea-03748551**

**<https://cea.hal.science/cea-03748551>**

Submitted on 9 Aug 2022

**HAL** is a multi-disciplinary open access archive for the deposit and dissemination of scientific research documents, whether they are published or not. The documents may come from teaching and research institutions in France or abroad, or from public or private research centers.

L'archive ouverte pluridisciplinaire **HAL**, est destinée au dépôt et à la diffusion de documents scientifiques de niveau recherche, publiés ou non, émanant des établissements d'enseignement et de recherche français ou étrangers, des laboratoires publics ou privés.

Article

# Effect of Sulfuric Acid Patination Treatment on Atmospheric Corrosion of Weathering Steel

Ana Crespo <sup>1</sup>, Iván Díaz <sup>1,\*</sup>, Delphine Neff <sup>2</sup>, Irene Llorente <sup>1</sup>, Sagrario Martínez-Ramírez <sup>3</sup>  
and Emilio Cano <sup>1</sup>

<sup>1</sup> Department of Surface Engineering, Corrosion and Durability, National Centre for Metallurgical Research (CENIM) Spanish National Research Council (CSIC), 28040 Madrid, Spain; a.crespoibanez@cenim.csic.es (A.C.); irene@cenim.csic.es (I.L.); ecano@cenim.csic.es (E.C.)

<sup>2</sup> DeIRAMIS/LAPA, CEA Saclay, 91911 Gif-sur-Yvette, France; delphine.neff@cea.fr

<sup>3</sup> Institute for the Structure of Matter (IEM) Spanish National Research Council (CSIC), 28006 Madrid, Spain; sagrario@iem.cfm.csic.es

\* Correspondence: ivan.diaz@csic.es; Tel.: +34-91-5538900

Received: 3 April 2020; Accepted: 28 April 2020; Published: 30 April 2020



**Abstract:** The requirements for the formation of a protective patina on conventional weathering steels (WS) are well known in the scientific literature related to civil structures. However, these criteria are not always given due consideration when WS is used in cultural heritage, as in the case of sculptural work. An artificial patina was produced simulating artists' working procedures using a direct patination technique, applying a solution of 10% H<sub>2</sub>SO<sub>4</sub> on WS specimens. These were exposed for two years in the urban atmosphere of Madrid along with weathering steel specimens without artificial patina, called natural patina. The patinas generated have been analyzed using colorimetry, micro-Raman spectroscopy, scanning electron microscopy (SEM), X-ray diffraction (XRD) and thickness measurements. The artificial patina color formed hardly differs from the color that the natural patina acquires from practically the beginning of its formation in the atmosphere of Madrid. After two years, the atmospheric corrosion rate of patinated WS is lower than 6 μm/year. The sulfuric acid treatment accelerates the protective ability of the patina with respect to the natural patina according to the ratio goethite to lepidocrocite (α/γ). Chromium-rich goethite is located in the inner part of the artificial patina as well as chromium-rich ferrihydrite. Ferrihydrite may act as a precursor of nanophasic goethite.

**Keywords:** weathering steel; atmospheric corrosion; artificial patina; natural patina; color; conservation; sculpture; ferrihydrite; chromium; micro Raman

## 1. Introduction

Weathering steel (WS), also known by its trade name COR-TEN, is a widely used material in civil engineering for buildings such as bridges, power poles or facades [1]. They are generally defined as low alloy steels with a total content of alloying elements (Cr, Ni, Cu and P) not higher than 5% weight [2], with an increased mechanical resistance and the protective effect that rust develops against atmospheric corrosion. Over time a stratified rust forms with two sublayers: an outer layer composed mainly of lepidocrocite, which is porous and not very compact, and an inner layer consisting of chromium-rich goethite of nanophasic size with sufficient compactness to exert a barrier effect and hinder the access of electrolyte to the steel/rust interface [3].

The requirements for the formation of a protective rust on conventional WS are well known in the scientific literature related to civil structures. Wet/dry cycles and moderate aggressivity atmospheres with low time of wetness and low levels of chlorides (<6 mg Cl<sup>-</sup>/m<sup>2</sup>d) and SO<sub>2</sub> (<20 mg/m<sup>2</sup>d) are

necessary to obtain allowable corrosion rates for bare WS [4]. In addition, the presence of sheltered zones and cavities that allow for the accumulation of water should be avoided in the structural design stage [5].

Technological advances have influenced artistic movements in the search for new materials for the creation of artworks. The use of WS in sculpture began in the early 1960s. Artists were looking for new materials with a durability similar or even greater than copper alloys from the atmospheric corrosion point of view [6]. The bright and lively colors of the rust make this steel a very aesthetic material with shades ranging from orange to violet, passing through yellow or brown [7]. Some artists have made WS a very recognized material in contemporary art, as is the case with Richard Serra, with art installations and public art all over the world.

However, engineering criteria are not always taken into consideration when WS is used in cultural heritage, as is the case of sculptural work. In these cases, the main criterion should be the creative vision of the artist. Both the exposure conditions and the design of the artwork are conditioned by artistic reasons rather than material durability. Thus, there are WS works in places not recommended for applications in civil structures, such as *Peine del Viento XV* by Eduardo Chillida, located offshore, just a few meters from the coast [8], or *East-West/West-East* by Richard Serra installed in the middle of the desert in Qatar [9]. There can also be interstices and cavities designed in the artwork that may hinder proper drying of the metal surface. This is the case of the artwork *Head n°2* by Naum Gabo [10] or *Cometh the Sun* by Curtis Paterson [11], which suffered premature deterioration requiring conservation-restoration interventions.

Another difference in the artistic application of WS with respect to its use in civil structures is the creation of artificial patinas by chemical treatments as part of the creative process of the work. Artists investigate different methods of creation with chemicals, testing salts and acids to obtain the colors and aesthetics that best fit their artistic intention before atmospheric exposure [12]. However, the subsequent effect of these treatments on the formation of protective rust is unknown. The conditions of application of these treatments are very personal since each artist develops their own methods of patination according to the aesthetics of their work.

Due to all the above mentioned issues, the conservation of artworks using WS has become a major concern among conservators-restorers. A growing number of research groups are delving into existing problems for the safeguard of WS artworks. For instance, Raffo et al. focused on rainwater runoff and dissolved ions from corroding WS as a potential source of pollution [13]. Travassos et al. quantified patina thicknesses in the steady state of WS using non-destructive methods (magnetic induction); they suggested that thickening rates of patinas lower than 2  $\mu\text{m}/\text{year}$  could be used as an evaluation method of WS sculptures in good conservation status [14]. Grassini et al. [15] and Angelini et al. [16] analyzed electrochemical properties of patinas using electrochemical impedance spectroscopy (EIS) for the same purpose. Aramendia et al. [17–19] studied the influence of marine and urban pollutants in the conservation of several artworks exposed to Bilbao atmosphere (Spain).

However, none of these studies has dealt with the effect of chemical treatments for artificial patination applied to WS artworks. Advance in this knowledge is necessary to ensure proper conservation and to highlight potential dangers to safeguard their future. Therefore, the aim of this paper is to study the consequences in terms of atmospheric corrosion arising from applying one of the most common chemical treatments in contemporary art used by sculptors to obtain artificial patinas on WS. After consulting a set of Spanish sculptors with WS artworks, application of dilute sulfuric acid (10%) was identified as one of the most common methods and selected as artificial treatment of patination for this study [20]. Once applied on WS specimens, a two-year atmospheric exposure test was performed in Madrid. An evolution of the artificial patina was assessed in terms of corrosion rate and compared with respect to a patina formed without chemical treatment. Their composition was characterized using scanning electron microscopy (SEM-EDX), X-ray diffraction (XRD) and Raman spectroscopy, paying special attention to the presence of ferrihydrite, a poorly crystalline oxyhydroxide

of difficult characterization typically related to the initial stage of atmospheric corrosion. Finally, color measurements of the patinas were performed to evaluate their aesthetic appearance.

## 2. Materials and Methods

### 2.1. Material

Specimens of a commercial weathering steel (WS) commonly used in the manufacture of sculptures were prepared by cutting from hot rolled sheets with final dimensions of 110 mm × 60 mm × 2 mm. Table 1 shows their chemical composition, which was obtained using arc/spark optical emission spectrometry with a SPECTROMAXx surface analyzer (SPECTRO Analytical Instruments GmbH, Kleve, Germany). The carbon and sulfur content was analyzed with a Leco model CS230 (Leco Corporation, St. Joseph, MI, USA) unit by combustion of a 5 g shaving of the material in an induction furnace and subsequent determination by infrared absorption.

**Table 1.** Chemical composition (wt. %) of the used weathering steel (WS).

Weathering Steel	C	Si	Mn	P	S	Cu	Cr	Ni	Al
ASTM A242	0.091	0.60	0.42	0.109	0.0123	0.302	0.807	0.181	0.025

Before atmospheric exposure, specimens were sandblasted with corundum (0.3–0.425 mm) to completely remove the oxide layer (mill scale) obtaining a surface finish of A Sa3 (bare metal), in accordance with Swedish standard SIS 055900. They were then cleaned in an ultrasonic bath, being submerged consecutively in distilled water, ethanol and acetone for 1 min in each solvent and then immediately dried with forced hot air and weighed in an analytical balance of 0.1 mg sensitivity.

The artificial patina was produced simulating artists' working procedures using a direct patination technique. A solution of 10% H<sub>2</sub>SO<sub>4</sub> was applied by brush covering the entire surface of the WS specimens with a single pass, and then they were air dried for 24 h. They were then washed once a day for a week spraying abundant distilled water to remove acid residues and allowed to air dry.

Parts of the specimens were taken prior to the atmospheric exposure test to analyze the artificial patina created. The rest of the specimens were used for the atmospheric exposure test.

### 2.2. Atmospheric Corrosion Test

Patinated and non-patinated WS specimens were exposed to the Madrid (Spain) atmosphere on a corrosion rack in March 2017 (Figure 1). The non-patinated WS samples, i.e., bare WS without artificial patina, were exposed to compare the artificial patina of 10% H<sub>2</sub>SO<sub>4</sub> with a natural patina developed without any previous chemical treatment. According to ASTM G50, the rack was placed facing south and at an angle of 45° from the horizontal plane [2]. Batches of five samples were withdrawn after 1 and 2 years of exposure in order to obtain data on mass loss due to corrosion following standard ISO 8407 (3 specimens) and for characterization of the patinas formed (2 specimens). Additional batches were withdrawn at 3 and 6 months to monitor the color changing.

Zero-time corrosion data correspond to the initial WS corrosion caused by the chemical treatment of 10% H<sub>2</sub>SO<sub>4</sub> prior to its atmospheric exposure.

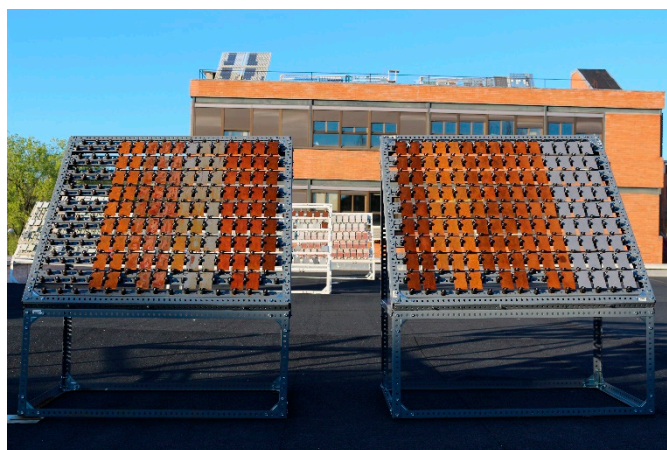


**Figure 1.** Atmospheric corrosion station located in Madrid (Spain).

The Madrid atmosphere is an urban atmosphere of corrosivity category C2, for low carbon steel, according to ISO 9223 [21]. Figure 2 shows monthly data on the relative humidity and temperature of Madrid from March 2017 to March 2019 supplied by the National Meteorological Institute (AEMET) of Spain. Therefore, Madrid had a dry climate during the study of this research with a moderate relative humidity and warm temperature especially in the summer.

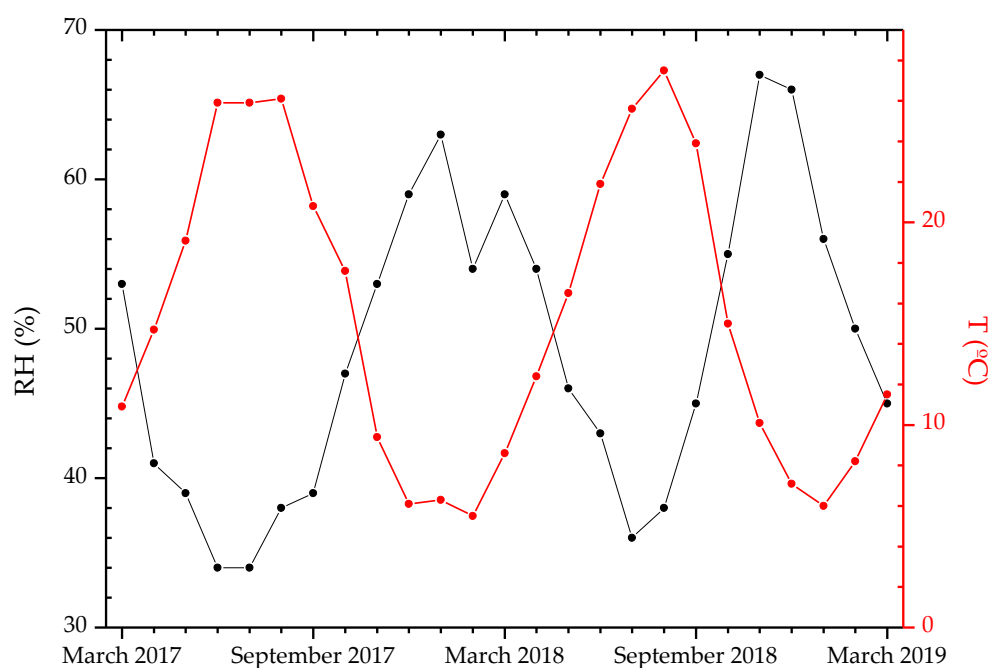


**Figure 2.** Monthly data of Madrid on relative humidity and temperature supplied by the National Meteorological Institute (AEMET) of Spain.

### 2.3. Characterization of Patinas

#### 2.3.1. Color Measurements

Since the goal of the studied WS is its application in sculptures, the aesthetics of its patina must be taken into account. After 0, 3, 6, 12 and 24 months of atmospheric exposure, the patina color was measured in the CIEL\*a\*b color space with a Konica Minolta CM-700d spectrophotometer (Konica Minolta Sensing Europe B.V., Nieuwegein, The Netherlands). All measurements were performed in

triplicate and averaged from 23 points evenly distributed over the patina surface of each specimen with D65 illuminant and in Specular Component Included mode.

### 2.3.2. Techniques of Chemical Analysis

Surface and cross sectional analyses of patinated and non-patinated WS specimens were performed after 1 and 2 years of exposure to the Madrid atmosphere.

#### Micro-Raman Spectroscopy

Surface analysis spectra were carried out with a RM 2000 Renishaw Raman microscope (Renishaw plc, Old Town, Wotton-under-Edge, Gloucestershire, UK) equipped with a laser at 633 nm with a spot diameter of 1  $\mu\text{m}$  and a Leica microscope coupled with an electrically refrigerated charge-coupled device (CCD) camera. The laser power was controlled at 2.5 mW in order to avoid thermal transformation [22]. Spectra were collected with 10 s of integration time and 5 accumulations to improve the signal-noise ratio.

Micro-Raman spectroscopy in cross section was performed using Renishaw Invia equipment (Renishaw plc, Old, Town, Wotton-under-Edge, Gloucestershire, UK) with a 532 nm Nd: YAG laser equipped with a Leica microscope. The diameter of the focus area was 1  $\mu\text{m}$ . The space resolution of the spectrometer is less than 2  $\text{cm}^{-1}$ . The power of the laser was no higher than 80  $\mu\text{W}$  to avoid thermal phase transition. Punctual spectra were performed with 50 s of acquisition; mapping was performed with 20 s of acquisition and 1  $\mu\text{m}$  spacing. In order to select a representative area of the patina for Raman mapping, previous spectra were performed all along the cross section of the rust.

Acquisition and phase assignment were done with WIRE (v. 3.4, Renishaw plc) and Multicorr software, which was developed at the Laboratoire "Archéomatériaux et Prévision de l'Altération" (LAPA) [23]. Mutlicorr software calculates principal component analysis (PCA), a commonly used algorithm for data mining. In our study, the data treatment is based on the calculation of spectral components supporting the maximum of information by the maximization of the covariance on a Raman map dataset. The projection of the first components are represented as map images. From these results a clustering method (K-means method) has been applied to emphasize the distribution of these components on the Raman map. At last, thanks to this operation, a reconstituted image of the predominance domain of each characteristic phase was drawn and is presented as a synthetic result for each sample in the results section. For correct phase assignment and data treatment using Multicorr, prior treatments of the spectra are necessary: (1) cosmic rays were removed using the nearest neighboring method; (2) all spectra were normalized in order to eliminate the effect of the intensity of the signal from the PCA, but no base line treatment was performed as the relative intensity of the Raman signal could be affected; (3) spectra from the base metal and resin were removed from the map data; and (4) PCA and clustering analysis was performed in the Raman spectra of the mapping.

#### Scanning Electron Microscopy (SEM)

The same cross-sectional areas of the patinas that were mapped using Raman spectroscopy were analyzed using a Jeol JSM 7001F SEM instrument (JEOL Ltd., Tokyo, Japan) equipped with secondary backscattered electron detectors. Energy dispersive spectroscopy (EDS) was also performed with Oxford Aztec software (v. 2.2 Oxford Instruments plc) attached to the SEM working at an accelerating voltage of 15 kV and using a silicon drift detector.

#### X-ray Diffraction (XRD)

X-ray diffraction (XRD) measurements were carried out using a Bruker AXS D8 diffractometer (Bruker AXS GmbH, Karlsruhe, Germany) equipped with a Co X-ray tube (wavelength 1.790  $\text{\AA}$ ) with Goebel mirror optics to obtain a parallel monochromatic X-ray beam. A current of 30 mA and a voltage of 40 kV were employed as tube settings. Due to the variable thickness of the patinas, XRD measurements were conducted in grazing incidence condition (GIXRD) and in conventional Bragg-Brentano geometry for  $2\theta$  scans ranging from 10 to 80° with a step width of 0.03° and a counting

time of 3 s/step. The appearance of the Fe peak in the diffractograms indicated that the analysis included the entire thickness of the patina. In order to quantify the proportion of the different phases presented in the patina, the Rietveld method was used with version 4.2 of the TOPAS (Bruker AXS GmbH, Karlsruhe, Germany) Rietveld analysis program and the crystallographic information obtained from the Pearson's crystal structure database.

### 2.3.3. Thickness Measurements

Patina thicknesses were measured with an Elcometer 456 Coating Thickness Gauge (Elcometer Ltd., Manchester, UK) equipped with an induction probe for ferrous substrates. Measures were taken in quintuplicate at fifteen points evenly distributed over the patina surface.

## 3. Results

### 3.1. Color Measurements

Figure 3 shows the chromaticity ( $a^*$  and  $b^*$ ) and lightness ( $L^*$ ) values obtained in the CIEL\*a\*b\* color space for the different patinas (with and without the chemical treatment of 10%  $H_2SO_4$ ) after 0, 3, 6, 12 and 24 months of exposure to the Madrid atmosphere. The chromaticity values ( $a^*$  and  $b^*$ ) have been grouped in circles. The blue circle indicates the initial state of the artificial patina before being exposed to the atmosphere (zero time). The green circle groups natural and artificial patinas after 3 and 6 months of exposure, while the red circle represents the same but for patinas after 12 and 24 months of exposure.

The lightness value,  $L^*$ , represents how light or dark a color is, being pure black at 0 and pure white at 100; the chromaticity  $a^*$  axis goes from red (+60) to green (−60), while the chromaticity  $b^*$  axis goes from yellow (+60) to blue (−60).

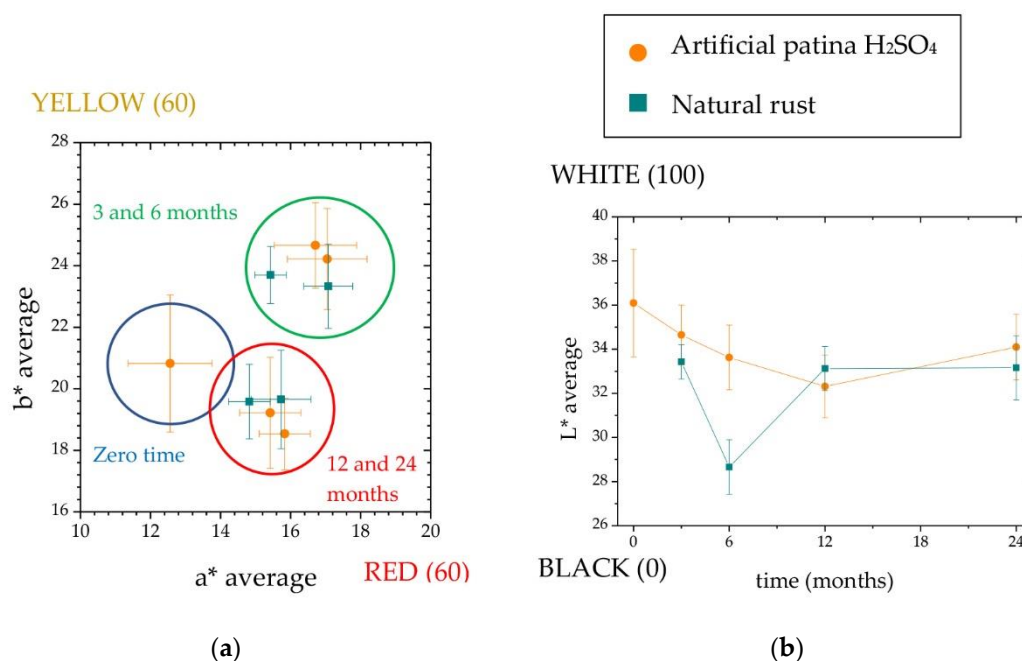


**Figure 3.** Values of the CIEL\*a\*b\* color space. (a) Chromaticity  $a^*$  and  $b^*$ ; (b) lightness  $L^*$ .

After three months of atmospheric exposure, the chromaticity values ( $a^*$  and  $b^*$ ) of both patinas increased slightly, the color of both patinas tending towards brighter orange hues. However, after 12 months of exposure and until the end of the atmospheric test, the chromaticity values returned to a position similar to the initial state from which the artificial patina started.

As for the luminosity, it remains practically constant throughout the atmospheric exposure with respect to the initial artificial patina. Only after six months of exposure, the natural patina darkens slightly compared to the artificial patina. However, this trend does not continue over time. As with the chromaticity values, after six months the lightness tends to return to the initial values of the fresh artificial patina.

Differences in color were calculated with  $\Delta E$  (Equation (1)), which indicates whether two colors are perceived as different to the human eye.  $\Delta E$  values are smaller than 5 (Table 2), except for six months, due to the darkening of the natural patina (Figure 3), which shows small differences in color.

$$\Delta E = \sqrt{(L_1^* - L_2^*)^2 + (a_1^* - a_2^*)^2 + (b_1^* - b_2^*)^2} \quad (1)$$

**Table 2.** Values of  $\Delta E$  calculated for the artificial and the natural patina.

Time of Exposition	$\Delta E$ Value
3 months	2.01
6 months	5.05
12 months	1.67
24 months	1.08

### 3.2. Atmospheric Corrosion Measurements

Figure 4 shows the corrosion evolution over time of exposure, in thickness loss, calculated from mass loss, for both the patinated WS with 10%  $H_2SO_4$  and the WS without artificial patina. As can be seen, the chemical treatment of 10%  $H_2SO_4$  applied before atmospheric exposure causes a 2.39  $\mu m$  thickness loss of WS.

After 24 months of exposure, the corrosion rate of the artificially patinated WS decreased by approximately 42% over the first year of exposure, reaching a final corrosion rate of 4.7  $\mu m/year$ . The corrosion rate of the non-patinated WS, i.e., with natural patina, also decreased progressively. However, the decrease was somewhat lower, around 25%, reaching a final corrosion rate of 4.22  $\mu m/year$ .

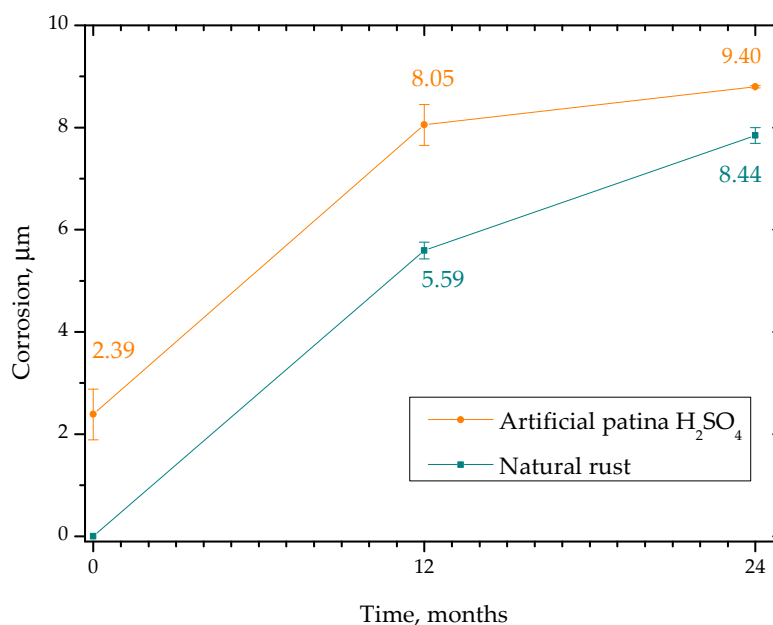


**Figure 4.** Corrosion versus time plot for both patinated WS with 10%  $H_2SO_4$  and bare WS without artificial patina exposed to the Madrid atmosphere. Figures in orange represent quantified corrosion for patinated WS, while the blue ones represent those of non-patinated WS.

### 3.3. Micro Raman Spectroscopy

#### 3.3.1. Surface Analysis

Figure 5a shows representative micro-Raman spectra of the artificial patina (10% H<sub>2</sub>SO<sub>4</sub>) and the natural patina formed on WS during its atmospheric exposure in Madrid for two years. Wavenumber shifts and relative intensities of Raman signal peaks correspond to the profile of lepidocrocite ( $\gamma$ -FeOOH) for both patinas, with a more intense and characteristic signal at 250 cm<sup>-1</sup> and another signal of less intensity at 380 cm<sup>-1</sup> (see second row of Table 3). These signals are narrow and well defined, which indicates a high degree of crystallinity [24] and high concentration of lepidocrocite. However, in some more specific areas of both patinas and regardless of the exposure time, a signal appears at 720 cm<sup>-1</sup> as a shoulder of the signal at 650 cm<sup>-1</sup> (Figure 5b). It is a non-characteristic lepidocrocite signal that can be associated with other oxidized iron phases such as feroxyhyte ( $\delta$ -FeOOH), maghemite ( $\gamma$ -Fe<sub>2</sub>O<sub>3</sub>) or ferrihydrite (Fe<sub>5</sub>HO<sub>8</sub>·4H<sub>2</sub>O) with Raman signals in the previous wavenumber range (see third, fourth and fifth row of Table 3).

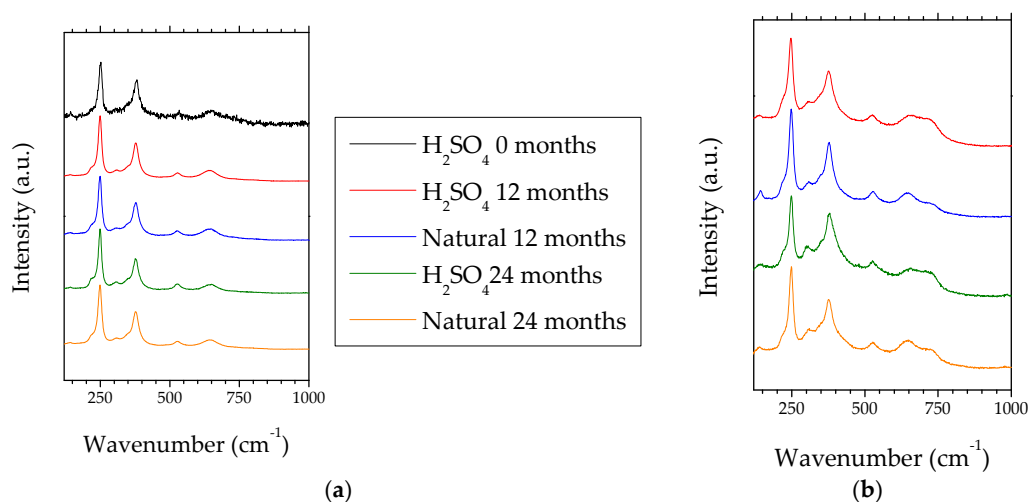


**Figure 5.** Raman spectra of artificial (10% H<sub>2</sub>SO<sub>4</sub>) and natural patinas formed on WS for 2 years at Madrid atmosphere, showing (a) characteristic peaks of lepidocrocite together with (b) less representative spectra with an additional signal at 720 cm<sup>-1</sup>.

**Table 3.** Characteristic wavelength shifts (cm<sup>-1</sup>) of the Raman peaks corresponding to lepidocrocite, feroxyhyte, maghemite and ferrihydrite found in different bibliographic sources. Main signal in bold.

Phases	Signals (cm <sup>-1</sup> )	References
Lepidocrocite ( $\gamma$ -FeOOH)	250, 306, 380, 525, 650	Actual data of our study
	<b>250</b> , 302, 343, 379, 525, 650	[25]
	<b>250</b> , 380, 650	[26]
	220, <b>250</b> , 309, 350, 377, 527, 648	[27]
	<b>250</b> , 300, 380, 525, 650	[28]
	<b>250</b> , 348, 379, 528, 650	[29]
Feroxyhyte ( $\delta$ -FeOOH)	400, <b>680</b>	[25]
	<b>680</b> , 1350	[26]
Maghemite ( $\gamma$ -Fe <sub>2</sub> O <sub>3</sub> )	380, 460, 510, <b>670</b> , <b>720</b>	[25]
	377, 510, <b>670</b> , <b>715</b>	[27]
	<b>670–720</b> , 1400	[26]
	380, 460, 510, <b>670</b> , <b>720</b> , 1160, 1400	[28]
	350, 512, <b>665</b> , <b>730</b>	[29]
Ferrihydrite (Fe <sub>5</sub> HO <sub>8</sub> ·4H <sub>2</sub> O)	370, 510, <b>710</b> , 1350	[25]
	361, 508, <b>707</b> , 1045	[30]
	370, 510, <b>710</b>	[29]
	370, 510, <b>710</b>	[31]

### 3.3.2. Cross Section Analysis

Figure 6 shows representative optical images of (a) the artificial patina just after applying the chemical treatment of 10%  $H_2SO_4$  on WS, prior to atmospheric exposure (zero time), (b) the artificial patina after 12 months of atmospheric exposure and, for comparative purposes, (c) the natural patina also after 12 months of atmospheric exposure.

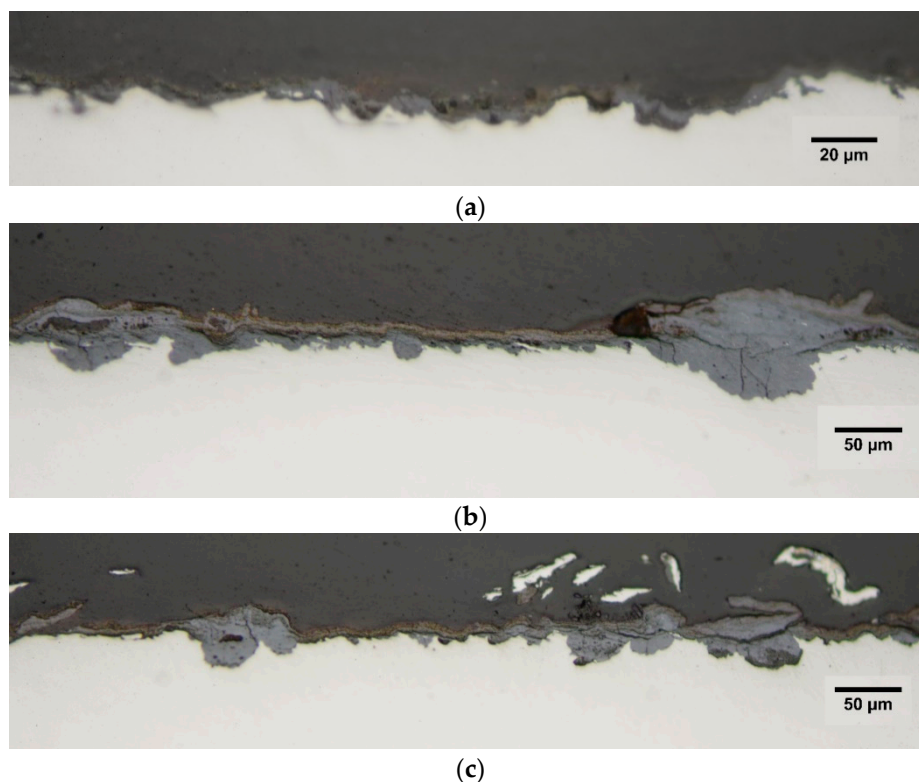


**Figure 6.** Optical microscope images showing evolution of the cross section of (a) the artificial patina (10%  $H_2SO_4$ ) from its initial formation on WS ( $t = 0$ ) and (b) after 12 months of exposure to the Madrid atmosphere. (c) Natural patina is shown for comparative purposes.

The cross section of the artificial patina at zero time is very thin with a homogeneous thickness of less than  $10 \mu m$ . It is not stratified and no preferential localized corrosion seems to be observed. After 12 months of atmospheric exposure, the artificial patina increases its thickness and stratifies into two layers: a thick gray inner layer and a thin outer layer of gray-orange color. In general, its thickness is quite uneven ranging from  $10$  to  $80 \mu m$ . The characteristics of the natural patina are quite similar with respect to the artificial patina at 12 months of exposure. It is also stratified, with thick and thin parts. However, its thickness is somewhat smaller.

The patina thicknesses (artificial and natural) at different times of exposure to the Madrid atmosphere were quantified using an induction probe, confirming the previous observations obtained from the optical microscope (Table 4).

**Table 4.** Thicknesses of patinas (average  $\pm$  SD) obtained after exposure to the atmosphere of Madrid.

Artificial Patina ( $t = 0$ )	Artificial Patina ( $t = 12$ months)	Natural Patina ( $t = 12$ months)
$6 \pm 1 \mu m$	$28 \pm 12 \mu m$	$20 \pm 9 \mu m$

A representative area of the cross section of the artificial patina ( $t = 0$ ) was selected to perform a compositional analysis using Raman mapping (Figure 7). A Raman spectrum is acquired every square micron of the scanned area showing different colors in areas depending on the patina composition.

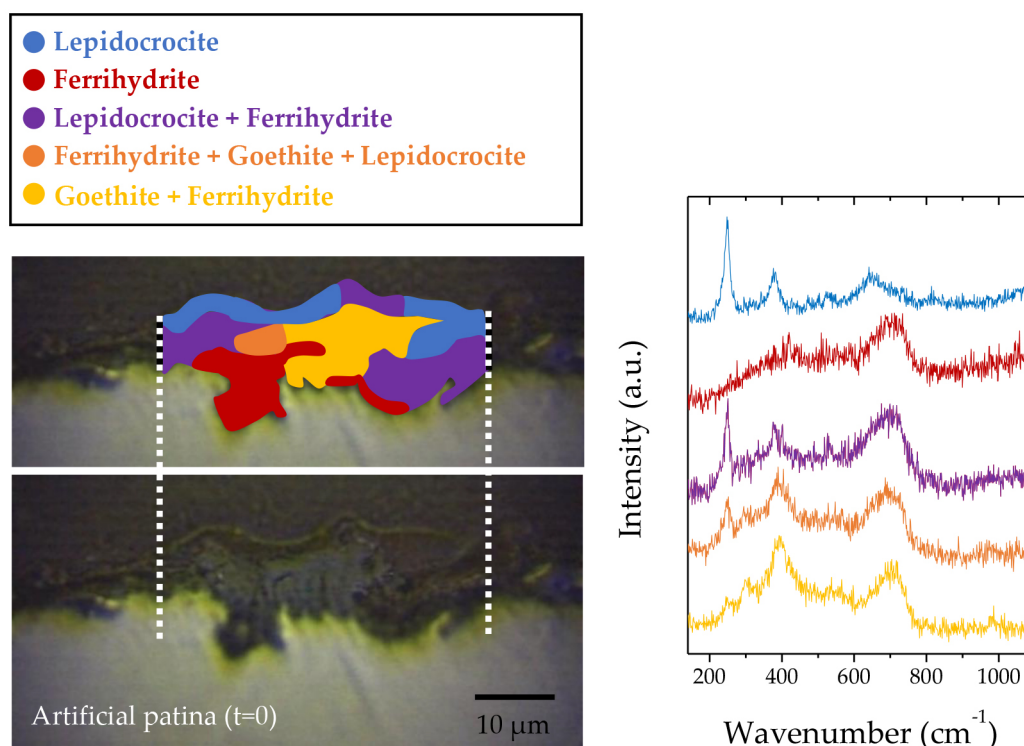


**Figure 7.** (a) Image of the phase distribution obtained using principal component analysis (PCA) data treatment from a Raman map acquired on the scanned cross section for the artificial patina (10% H<sub>2</sub>SO<sub>4</sub>) before atmospheric exposure; (b) Raman spectra of the different phases detected in the Raman map.

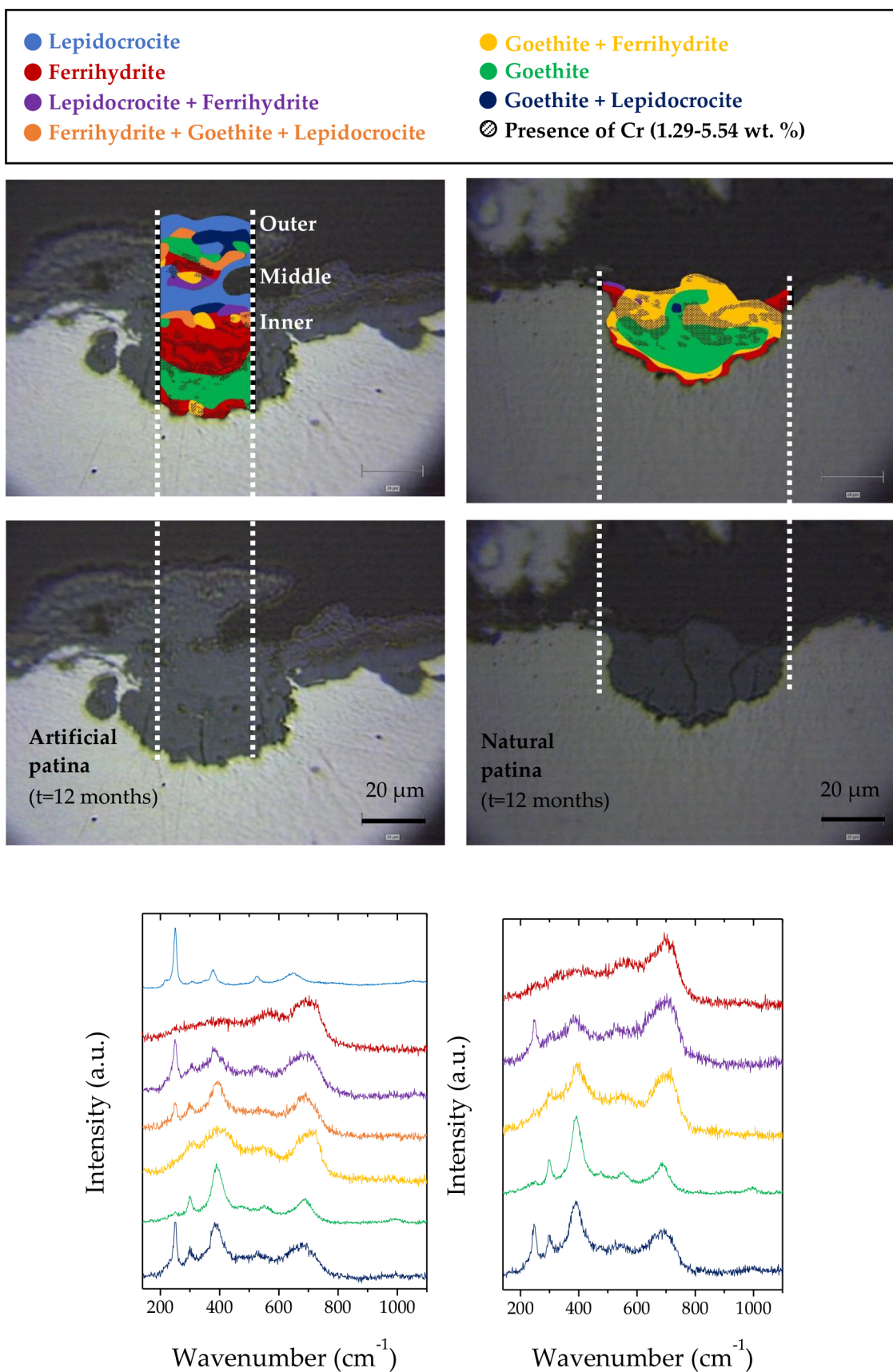
The ferrihydrite phase is identified and located mostly in the inner part of the artificial patina, near the patina/WS interface. Lepidocrocite is concentrated in the outer part of the artificial patina, confirming the results obtained by micro-Raman from surface analysis. In addition, lepidocrocite and ferrihydrite appear mixed both externally and internally in the patina, which can be in contact with the metal. They are probably in a transient reactive stage. Finally, goethite mixed with the previous phases is identified and located in the inner and middle part of the artificial patina and can be in contact with the metal as well.

Figure 8 comparatively shows Raman maps of the cross-sectional composition for the artificial and natural patina after 12 months of exposure to the atmosphere of Madrid. It also highlights the EDS analysis performed for the detection of chromium within the stratified patina.

The inner part of the artificial patina ( $t = 12$  months) consists of alternate layers of ferrihydrite and goethite. Chromium accumulates mostly in this part of the patina and ferrihydrite is in direct contact with the steel substrate.

In the middle part, there is mostly a lepidocrocite stratum along with a small ferrihydrite domain in which chromium also accumulates. The presence of cracks and pores facilitates the access of electrolyte and therefore the formation of new lepidocrocite.

As for the natural patina ( $t = 12$  months), the thick part is mainly composed of ferrihydrite and goethite, either independently or mixed. As before, chromium is concentrated in areas where ferrihydrite is present, even mixed with goethite. However, unlike artificial patina (12 months), chromium is not located where there is only goethite; the spectrum of this area indicates that the goethite is very pure and crystalline. Therefore, the formation of this goethite could be influenced by the presence of cracks rather than by phase transformation. Finally, traces of lepidocrocite appear on the outer part of the patina. It is likely that it was partially detached during sample preparation since it was frequently observed in other parts of the patina.



**Figure 8.** Raman map of the scanned cross sections after being exposed to the atmosphere of Madrid for 12 months with the corresponding Raman spectra of the principal components identified in the Raman map for (a) artificial patina and (b) natural patina.

### 3.4. X-ray Diffraction

Table 5 shows the evolution of the crystalline phases found in the artificial (10% H<sub>2</sub>SO<sub>4</sub>) and natural patina formed on WS exposed for 24 months to the atmosphere of Madrid. The entire thickness of both patinas was analyzed ensuring the presence of the ferrite peak from the metallic substrate (WS). A quantitative analysis of each detected phase was performed using the Rietveld method, expressed as a percentage of the total crystalline products found. To make the results comparable, the ferrite phase was eliminated and the proportion of the remaining phases were recalculated.

**Table 5.** Percentage of the identified phases determined using X-ray diffraction (XRD) results (Rietveld refinement) obtained from the artificial patina (10% H<sub>2</sub>SO<sub>4</sub>) and the natural patina exposed for two years to the atmosphere of Madrid.

Specimen	Lepidocrocite (%)	Goethite (%)	Spinel (%)
Artificial patina (t = 0)	70.32	17.58	12.39
Artificial patina (t = 12 months)	82.10	15.23	2.67
Artificial patina (t = 24 months)	76.90	19.31	3.80
Natural patina (t = 12 months)	89.41	8.30	2.40
Natural patina (t = 24 months)	82.37	14.15	3.28

There are three phases present in both patinas. The main phase in terms of content is lepidocrocite, followed by goethite and finally the minor phase of spinel. The spinel phase encompasses both magnetite and maghemite since these phases are indistinguishable using XRD [21]. None of these phases were identified using Raman spectroscopy. Only in the surface analysis of both patinas (artificial and natural), a signal at 720 cm<sup>-1</sup> not assigned to lepidocrocite could be assigned to maghemite (see Table 3).

The initial chemical treatment with 10% H<sub>2</sub>SO<sub>4</sub> generates an artificial patina with a relatively high content of goethite (17.58%); this content is even higher than that of the natural patina formed during 24 months in the atmosphere of Madrid. Once the patinated WS was exposed for one year to the Madrid atmosphere, the goethite content was slightly reduced. This could be related to a poor adherence of the patina formed quickly by the chemical treatment or by an increase in the lepidocrocite content with respect to goethite. Subsequently, after two years of exposure, the content of goethite increases again following the typical behavior of bare WS exposed to an urban atmosphere such as Madrid. This was also the case with the evolution of the natural patina formed on WS.

## 4. Discussion

The application of chemical treatments to generate artificial patinas on WS is a procedure used by sculptors to simulate patina colors formed during long-term atmospheric exposures. The artificial patina color formed with 10% H<sub>2</sub>SO<sub>4</sub> hardly differs from the color that the natural patina acquires from practically the beginning of its formation in the atmosphere of Madrid. The chromaticity and luminosity values of the samples with artificial and natural patina are almost identical after three months of exposure (first measurement performed). Sculptors quickly achieve the aesthetics that nature takes months to generate. However, the use of sulfuric acid that leads to the artificial patina formation initially implies additional corrosion. Specifically, it caused a thickness loss of WS of 2.39 μm prior to atmospheric exposure. This initial corrosion would be similar to that experienced by bare WS exposed for a year to a rural atmosphere. Although it is a patination treatment of low corrosivity, the ions in which the sulfuric acid dissociates (H<sup>+</sup> and SO<sub>4</sub><sup>2-</sup>) could affect the subsequent corrosive process and, therefore, the long-term development of a protective rust in the atmosphere.

There are several criteria to assess the state of conservation of WS exposed to the atmosphere. One of them is to use the engineering criteria [2]. The atmospheric corrosion rate of WS must be ≤ 6 μm/year for its use without paint coatings to be advised. After two years of atmospheric exposure, the corrosion rate of artificially patinated WS with sulfuric acid was 4.7 μm/year. This was slightly

higher than the corrosion rate experienced by the WS without artificial patina, 4.22  $\mu\text{m}/\text{year}$ . Therefore, the patination of WS with 10%  $\text{H}_2\text{SO}_4$  does not seem to compromise the material durability when exposed to the atmosphere of Madrid. In just two years of exposure, it reached a tolerable rate of atmospheric corrosion that would allow optimal conservation of WS. The atmosphere of Madrid through successive rain-washes allows the removal of possible traces of the acid patination treatment. In addition, there was no corrosive source of pollution nearby. It is an urban atmosphere with low levels of  $\text{SO}_2$  (0.8  $\text{mg}/\text{m}^2\text{d}$ ) located 360 Km from the nearest coast.

Another alternative is to use protective ability indexes that evaluate how protective a patina formed in the atmosphere is on WS based on its composition determined using XRD. Yamashita et al. [32] found that the corrosion rate of WS exposed to rural and industrial atmospheres decreased as the mass ratio of goethite to lepidocrocite ( $\alpha/\gamma$ ) increased. They considered  $\alpha/\gamma > 2$  to be an indication of obtaining a protective patina after decades of atmospheric exposure [33]. Later, other research groups modified the protective ability index proposed by Yamashita based on the thermodynamic stability of newly identified phases of iron oxides and oxihydroxides. For instance, Dillmann et al. proposed adding the magnetite content to the numerator of the previous index from old rusts and considering this as protective despite the fact that is a conducting phase [34]. Both protective ability indexes were calculated for the artificial and natural patina with respect to the exposure time in the atmosphere of Madrid. However, since the amount of quantified spinel in the different patinas is relatively small, the protective ability indexes were very similar. Hence, Figure 9 shows only the results of the  $\alpha/\gamma$  index. None of the patinas had a goethite content high enough to be greater than twice the lepidocrocite content ( $\alpha/\gamma > 2$ ). They need more exposure time to achieve that situation since the corrosion rate of WS has not yet reached the steady state. However, nothing suggests that the artificial patination precludes the above from happening.

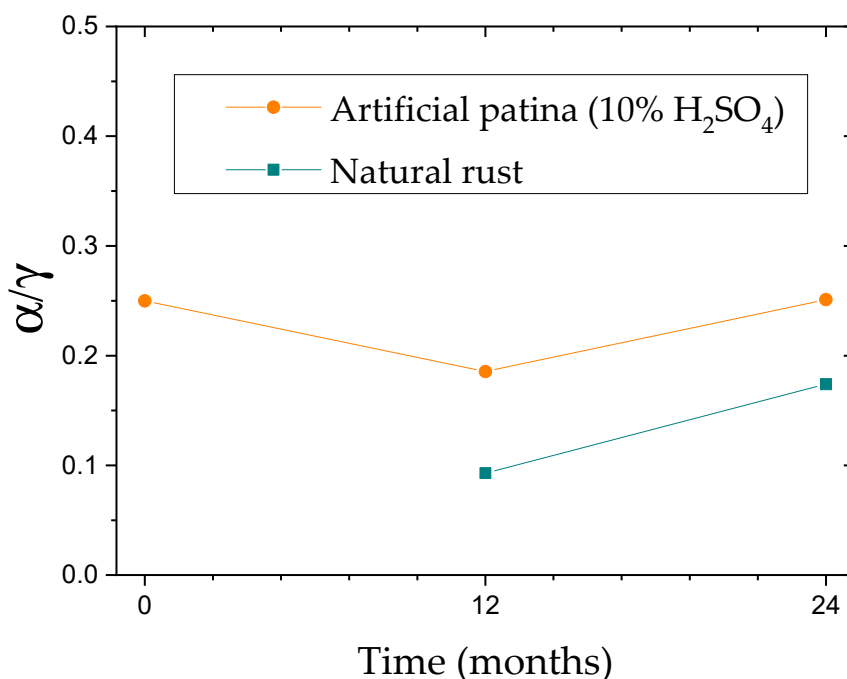


**Figure 9.** Evolution with exposure time of the  $\alpha/\gamma$  ratio for the artificial and natural patina exposed to the atmosphere of Madrid for 24 months.

The artificial patination treatment of 10%  $\text{H}_2\text{SO}_4$  has an  $\alpha/\gamma$  index close to the same as for artificial patination after 24 months of atmospheric exposure. It decreased after 12 months of atmospheric exposure but the  $\alpha/\gamma$  ratio continued above that of the natural patina. During the initial atmospheric corrosion mainly lepidocrocite is formed, therefore the index decreases. Later, after 24 months of atmospheric exposure the  $\alpha/\gamma$  ratio increased as expected. This was the behavior shown by the natural

patina from the beginning of exposure. Lepidocrocite is progressively transformed into goethite via dissolution and precipitation during wet/dry cycles in the atmosphere.

In a certain way, the sulfuric acid treatment increases the protective ability of the patina because its  $\alpha/\gamma$  ratio after 12 months of atmospheric exposure is similar to that of the natural patina after 24 months of exposure.

A necessary but not sufficient condition for the formation of a protective patina on WS is its stratification into two sublayers. The additional condition is that the inner layer must be rich in goethite while the outer layer in lepidocrocite. From the optical images in Figure 6, the artificial patina just after its formation (zero time) does not seem to be stratified since its thickness is very thin, less than 10  $\mu\text{m}$ ; it is a patina with little quantity of corrosion products to stratify. Nevertheless, it is possible to distinguish two different parts (outer and inner) according to the location of the phases. As for its composition, Table 6 shows a summary of it within the patina.

**Table 6.** Summary of the localization of the different identified iron phases within the artificial patina at zero time. L means lepidocrocite, F, ferrihydrite and G, goethite.

Part of the Patina	L	F	L + F	G + F	G + F + L
Outer part	Yes	-	Yes	-	-
Inner part	-	Yes	Yes	Yes	Yes

The goethite phase found is not pure in the inner part of the patina but mixed with ferrihydrite and lepidocrocite phases. Pure ferrihydrite is also located in the inner part of the patina. Finally, pure lepidocrocite is located in the outer part of the patina, while it is mixed with ferrihydrite both externally and internally in the patina. The rapid oxidation of the patination treatment on WS generates mixed phases, although mostly goethite is located in the inner part of the patina and lepidocrocite in the external part. After 12 months of exposure to the atmosphere of Madrid, the patina thickness increases (around 28  $\mu\text{m}$ ) and stratifies. Lepidocrocite is mainly concentrated in the middle and outer part of the patina, while goethite and ferrihydrite are alternated within the inner layer [1]. It is in this part where chromium has accumulated, which is associated with the formation of nanophasic goethite, that a greater protective effect is exerted [32,35]. Therefore, it can be affirmed that the 10%  $\text{H}_2\text{SO}_4$  treatment of patination applied on WS exposed to the urban atmosphere of Madrid generates a patina that evolves normally towards a protective patina and that does not compromise the WS preservation.

On the other hand, ferrihydrite was detected using Raman spectroscopy along with the different phases of iron commonly identified using XRD. It is usually found on the inner part of the artificial and natural patina and mostly in direct contact with the WS metal substrate. It is a fact to highlight because it is a difficult phase to identify when it naturally forms in the atmosphere within the set of corrosion products. It has a low particle size, which makes it go unnoticed in XRD analysis, being appreciated as amorphous. In addition, its high thermodynamic instability allows it to transform into more stable and crystalline oxides, mainly goethite and hematite. Cornell and Schwertmann describe the competitive mechanism that leads to goethite or hematite formation [36]. At acidic pH and moderated temperature, the dissolution of ferrihydrite occurs and precipitates to goethite. However, hematite requires neutral pHs and high temperature. Since the presence of hematite in atmospheric corrosion products is minor, ferrihydrite could be an excellent precursor of nanophasic goethite, which is mostly concentrated in the inner layer of a protective patina. Another fact to keep in mind is that chromium is also associated with the presence of ferrihydrite as well as being nanophasic of a protective patina formed during years of atmospheric exposure.

## 5. Conclusions

The different characterization techniques reveal that there are no significant differences in composition between the natural and the artificial patina formed by accelerating the corrosion process

using 10% sulfuric acid. Furthermore, some aesthetical properties such as color are very similar in both cases.

After two years of exposure, the artificial accelerated patina seems to have a barrier effect which protects the base metal against atmospheric corrosion. Nevertheless, a longer exposure time is needed in order to compare the evolution of both natural and artificial accelerated patina and to verify the similarities between them.

It has been proved that using only one characterization technique is not enough for a complete characterization of the rust. For a proper identification of all the iron compounds, cross section analysis was necessary to complement the X ray diffraction results.

Among the phases characterized, ferrihydrite was detected in the inner part of the rust layer and associated with a high quantity of chromium. A hypothesis for this fact may be that ferrihydrite could be the precursor of the nanophasic goethite, as both of them were located in the inner part of the rust layer. They presented a small crystal size and were closely related to a high concentration of chromium [32,35].

As a whole, the artificial patination with 10% sulphuric acid seems a promising procedure for a quick development of the patina on works of art made of WS exposed to urban atmospheres.

**Author Contributions:** Conceptualization, A.C., I.D., D.N. and E.C.; methodology, A.C., I.D. and E.C.; validation, D.N., I.L. and S.M.-R.; formal analysis, A.C., I.D., I.L. and S.M.-R.; investigation, A.C. and I.D.; resources, I.D., D.N., I.L., S.M.-R. and E.C.; data curation, A.C., I.D., D.N., I.L. and S.M.-R.; writing—original draft preparation, A.C. and I.D.; writing—review and editing, A.C., I.D., D.N., I.L., S.M.-R. and E.C.; supervision, I.D., D.N., S.M.-R. and E.C.; project administration, I.D. and E.C.; funding acquisition, D.N., I.L., S.M.-R. and E.C. All authors have read and agreed to the published version of the manuscript.

**Funding:** This research was funded by Agencia Estatal de Investigación, grant number BES-2015-071472, and by Comunidad de Madrid and European Structural and Investment Funds, project TOP-HERITAGE CM (S2018/NMT-4372) and project GEOMATERIALES 2 (S2013/MIT-2914).

**Acknowledgments:** Authors would like to thank Mickael Bouhier and Robin Le Penglau for the development of the Multicorr software and their help in the analysis and Ana Ibáñez for her help with English corrections and are thankful for the professional support of the CSIC Interdisciplinary Thematic Platform from: Open Heritage Research and Society (PTI-PAIS).

**Conflicts of Interest:** The authors declare no conflict of interest.

## References

1. Morcillo, M.; Díaz, I.; Chico, B.; Cano, H.; de la Fuente, D. Weathering steels: From empirical development to scientific design. A review. *Corros. Sci.* **2014**, *83*, 6–31. [[CrossRef](#)]
2. Morcillo, M.; Chico, B.; Díaz, I.; Cano, H.; de la Fuente, D. Atmospheric corrosion data of weathering steels. A review. *Corros. Sci.* **2013**, *77*, 6–24. [[CrossRef](#)]
3. Qian, Y.; Ma, C.; Niu, D.; Xu, J.; Li, M. Influence of alloyed chromium on the atmospheric corrosion resistance of weathering steels. *Corros. Sci.* **2013**, *74*, 424–429. [[CrossRef](#)]
4. Morcillo, M.; Díaz, I.; Cano, H.; Chico, B.; de la Fuente, D. Atmospheric corrosion of weathering steels. Overview for engineers. Part I: Basic concepts. *Constr. Build. Mater.* **2019**, *213*, 723–737. [[CrossRef](#)]
5. Morcillo, M.; Díaz, I.; Cano, H.; Chico, B.; de la Fuente, D. Atmospheric corrosion of weathering steels. Overview for engineers. Part II: Testing, inspection, maintenance. *Constr. Build. Mater.* **2019**, *222*, 750–765. [[CrossRef](#)]
6. Scott, J. Conservation of weathering steel sculpture. In *Saving the Twentieth Century: The Degradation and Conservation of Modern Materials*; Canadian Conservation Institute: Ottawa, ON, Canada, 1991.
7. Gallagher, W.P. The Performance of Weathering Steel in Sculpture. *Mater. Perform.* **2001**, *40*, 58–61.
8. Arcaute, E.R.D. El Peine del Viento de Eduardo Chillida. Una revisión crítica de los estudios realizados para su conservación. In *Jornada de Conservación de Arte Contemporáneo*; Museo Nacional Centro de Arte Reina Sofía: Madrid, Spain, 2008.
9. Golfomitsou, S. The role of conservation in new contemporary art installations in new contexts: The case of Richard Serra's East–West/West–East in Qatar. *Stud. Conserv.* **2016**, *61*, 55–60. [[CrossRef](#)]

10. Pullen, D.; Heuman, J. Modern and Contemporary Outdoor Sculpture Conservation: Challenges and Advances. In *Conservation Perspectives*; The Getty Conservation Institute: Los Angeles, CA, USA, 2007.
11. Chemello, C.; Cano, E.; Crespo, A.; Mardikian, P.; Patterson, C. Conservation and Investigation of Cometh the Sun: A Monumental Corten Steel Sculpture. In Proceedings of the Interim Meeting of the ICOM-CC Metals Working Group, Neuchatel, Switzerland, 2–6 September 2019; International Council of Museums–Committee for Conservation (ICOM-CC) and Haute Ecole Arc Conservation-Restauracion (HE-Arc CR): Neuchatel, Switzerland, 2019.
12. Crespo, A.; Ramírez-Barat, B.; Díaz, I.; Cano, E. Efecto del patinado artificial en la conservación de escultura contemporánea de acero corten: Estudio de la obra Templo de Adriana Veyrat. In *Jornada de Conservación de Arte Contemporáneo*; Museo Nacional Centro de Arte Reina Sofia: Madrid, Spain, 2017; pp. 193–202.
13. Raffo, S.; Vassura, I.; Chiavari, C.; Martini, C.; Bignozzi, M.C.; Passarini, F.; Bernardi, E. Weathering steel as a potential source for metal contamination: Metal dissolution during 3-year of field exposure in a urban coastal site. *Environ. Pollut.* **2016**, *213*, 571–584. [[CrossRef](#)]
14. de Jesus Barradas Travassos, S.; de Almeida, M.B.; Tomachuk dos Santos Catuogno, C.R.; de Melo, H.G. Non-destructive thickness measurement as a tool to evaluate the evolution of patina layer formed on weathering steel exposed to the atmosphere. *J. Mater. Res. Technol.* **2019**, *9*, 687–699. [[CrossRef](#)]
15. Grassini, S.; Angelini, E.; Parvis, M.; Bouchar, M.; Dillmann, P.; Neff, D. An in situ corrosion study of Middle Ages wrought iron bar chains in the Amiens Cathedral. *Appl. Phys. A: Mater. Sci. Process.* **2013**, *113*, 971–979. [[CrossRef](#)]
16. Angelini, E.; Grassini, S.; Parvis, M.; Zucchi, F. An in situ investigation of the corrosion behaviour of a weathering steel work of art. *Surf. Interface Anal.* **2012**, *44*, 942–946. [[CrossRef](#)]
17. Aramendia, J.; Gomez-Nubla, L.; Bellot-Gurlet, L.; Castro, K.; Paris, C.; Colombar, P.; Madariaga, J.M. Protective ability index measurement through Raman quantification imaging to diagnose the conservation state of weathering steel structures. *J. Raman Spectrosc.* **2014**, *45*, 1076–1084.
18. Aramendia, J.; Gomez-Nubla, L.; Castro, K.; Madariaga, J.M. Structural and chemical analyzer system for the analysis of deposited airborne particles and degradation compounds present on the surface of outdoor weathering steel objects. *Microchem. J.* **2015**, *123*, 267–275. [[CrossRef](#)]
19. Aramendia, J.; Gomez-Nubla, L.; Castro, K.; Martinez-Arkarazo, I.; Vega, D.; Sanz López de Heredia, A.; García Ibáñez de Opakua, A.; Madariaga, J.M. Portable Raman study on the conservation state of four CorTen steel-based sculptures by Eduardo Chillida impacted by urban atmospheres. *J. Raman Spectrosc.* **2012**, *43*, 1111–1117. [[CrossRef](#)]
20. Crespo, A.; Ramírez-Barat, B.; Cano, E. Artificial patinas in contemporary weathering steel sculpture. In Proceedings of the V International Conference of Youth in Conservation of Cultural Heritage, Madrid, Spain, 21–23 September 2016.
21. Díaz, I. Corrosión Atmosférica de Aceros Patinables de Nueva Generación. Ph.D. Thesis, Departamento de Ciencia de los Materiales e Ingeniería Metalúrgica, Universidad Complutense de Madrid, Madrid, Spain, 26 October 2012.
22. Criado, M.; Martínez-Ramírez, S.; Bastidas, J.M. A Raman spectroscopy study of steel corrosion products in activated fly ash mortar containing chlorides. *Constr. Build. Mater.* **2015**, *96*, 383–390. [[CrossRef](#)]
23. Le Penglau, R. Analyses Multivariées et Multiblocs D’images Hyperspectrales Pour la Prédiction de la Corrosion sur le Long Terme: Application à la Corrosion Atmosphérique D’alliages Ferreux Historiques. Ph.D. Thesis, Laboratoire “Archéomatériaux et Prévision de l’Altératio” 2017et Sorbonne Universités, Paris, France, 12 December 2017.
24. Sklute, E.C.; Kashyapet, S.; Darby Dyar, M.; Holden, J.F.; Tague, T.; Wang, P.; Jaret, S.J. Spectral and morphological characteristics of synthetic nanophase iron (oxyhydr)oxides. *Phys. Chem. Miner.* **2018**, *45*, 1–26.
25. Neff, D.; Bellot-Gurlet, L.; Dillmann, P.; Reguer, S.; Legrand, L. Raman imaging of ancient rust scales on archaeological iron artefacts for long-term atmospheric corrosion mechanisms study. *J. Raman Spectrosc.* **2006**, *37*, 1228–1237. [[CrossRef](#)]
26. Colombar, P. Potential and Drawbacks of Raman (Micro) spectrometry for the Understanding of Iron and Steel Corrosion. In *New Trends and Developments in Automotive System Engineering*; Chiaberge, M., Ed.; IntechOpen: London, UK, 2001.

27. Nieuwoudt, M.K.; Comins, J.D.; Cukrowski, I. The growth of the passive film on iron in 0.05 M NaOH studied in situ by Raman micro-spectroscopy and electrochemical polarisation. Part I: Near-resonance enhancement of the Raman spectra of iron oxide and oxyhydroxide compounds. *J. Raman Spectrosc.* **2011**, *42*, 1335–1339. [[CrossRef](#)]
28. Froment, F.; Tournié, A.; Colomban, P. Raman identification of natural red to yellow pigments: Ochre and iron-containing ores. *J. Raman Spectrosc.* **2008**, *39*, 560–568. [[CrossRef](#)]
29. Hanesch, M. Raman spectroscopy of iron oxides and (oxy) hydroxides at low laser power and possible applications in environmental magnetic studies. *Geophys. J. Int.* **2009**, *177*, 941–948. [[CrossRef](#)]
30. Das, S.; Hendry, M.J. Application of Raman spectroscopy to identify iron minerals commonly found in mine wastes. *Chem. Geol.* **2011**, *290*, 101–108. [[CrossRef](#)]
31. Mazzetti, L.; Thistlethwaite, P.J. Raman spectra and thermal transformations of ferrihydrite and schwertmannite. *J. Raman Spectrosc.* **2002**, *33*, 104–111. [[CrossRef](#)]
32. Yamashita, M.; Miyuki, H.; Matsuda, Y.; Nagano, H.; Misawa, T. The long term growth of the protective rust layer formed on weathering steel by atmospheric corrosion during a quarter of a century. *Corros. Sci.* **1994**, *36*, 283–299. [[CrossRef](#)]
33. Yamashita, M.; Uchida, H. Recent Research and Development in Solving Atmospheric Corrosion Problems of Steel Industries in Japan. In *Industrial Applications of the Mössbauer Effect*; Springer: Dordrecht, The Netherlands, 2002.
34. Dillmann, P.; Mazaudier, F.; Hœrlé, S. Advances in understanding atmospheric corrosion of iron. I. Rust characterisation of ancient ferrous artefacts exposed to indoor atmospheric corrosion. *Corros. Sci.* **2004**, *46*, 1401–1429. [[CrossRef](#)]
35. Cook, D.C.; Oh, S.J.; Balasubramanian, R.; Yamashita, M. The role of goethite in the formation of the protective corrosion layer on steels. *Hyperfine Interact.* **1999**, *122*, 59–70. [[CrossRef](#)]
36. Cornell, R.M.; Schwertmann, U. *The Iron Oxides. Structure, Properties, Reactions, Occurrences and Uses*, 2nd ed.; WILEY-VCH: Weinheim, Germany, 2003.



© 2020 by the authors. Licensee MDPI, Basel, Switzerland. This article is an open access article distributed under the terms and conditions of the Creative Commons Attribution (CC BY) license (<http://creativecommons.org/licenses/by/4.0/>).